Ultra-wide patch antenna array design at 60GHz band for remote vital sign monitoring with doppler radar principle

Rabbani, Muhammad Saqib; Ghafouri-shiraz, Hooshang

DOI:
10.1007/s10762-016-0344-z

Document Version
Publisher's PDF, also known as Version of record

Citation for published version (Harvard):
Rabbani, MS & Ghafouri-shiraz, H 2017, 'Ultra-wide patch antenna array design at 60GHz band for remote vital sign monitoring with doppler radar principle', *Journal of Infrared, Millimeter, and Terahertz Waves*, vol. 38, no. 5, pp. 548–566. https://doi.org/10.1007/s10762-016-0344-z

J Infrared Milli Terahz Waves
DOI 10.1007/s10762-016-0344-z

Ultra-Wide Patch Antenna Array Design at 60 GHz Band for Remote Vital Sign Monitoring with Doppler Radar Principle

Muhammad Saqib Rabbani[1] · **Hooshang Ghafouri-Shiraz**[1]

Received: 11 July 2016 / Accepted: 18 November 2016

Abstract In this paper, ultra-wide patch antenna arrays have been presented at 60 GHz band (57.24–65.88 GHz) with improved gain and beam-width capabilities for remote detection of respiration and heart beat rate of a person with Doppler radar principle. The antennas measured and simulation results showed close agreement. The breathing rate (BR) and heart rate (HR) of a 31-year-old man have been accurately detected from various distances ranging from 5 to 200 cm with both single-antenna and dual-antenna operations. In the case of single-antenna operation, the signal is transmitted and received with the same antenna, whereas in dual-antenna operation, two identical antennas are employed, one for signal transmission and the other for reception. It has been found that in case of the single-antenna operation, the accuracy of the remote vital sign monitoring (RVSM) is good for short distance; however, in the case of the dual-antenna operations, the RVSM can be accurately carried out at relatively much longer distance. On the other hand, it has also been seen that the visual results are more obvious with higher gain antennas when the radar beam is confined just on the subject's body area.

Keywords Microstrip antenna · Ultra-wide patch arrays · Remote vital sign monitoring · Doppler radar · Non-contact vital signs monitoring · 60 GHz antenna arrays

1 Introduction

Non-contact detection of respiration and heart beat rate with Doppler radar is a more convenient way to check the vitality signs of a person as compared to the conventional

✉ Hooshang Ghafouri-Shiraz
ghafourh@bham.ac.uk

Muhammad Saqib Rabbani
saqibrabbani05@hotmail.com

[1] School of Electronic Electrical and System Engineering, University of Birmingham, Edgbaston B15 2TT, UK

Published online: 20 December 2016

vital sign monitoring devices, such as electrocardiogram (ECG), pulse oximetry and capnography, because the conventional devices need direct sensors plantation on the subject body as well as they consume comparatively much longer implementation time to start the measurements [1–8]. However, the results accuracy and reliability of RVSM system need to be dealt appropriately for its real-life applications [2]. RVSM finds a vast number of applications in regular and special health care, emergency services, security and defence sectors [1–12].

In the recent couple of decades, a significant amount of research has been conducted to improve the accuracy of the RVSM by employing various techniques including distance and frequency optimization [13–18], robust signal processing methods [19–21], breath holding for HR detection and so on [22–28]. However, most of the reported practical work is based on Doppler radars working at lower microwave (MW) frequency bands around 2.4, 5.8 and 10 GHz where the wavelength resolution of the electromagnetic wave is low and therefore the accuracy of the vital signs detection, especially the HR, remained challenging [23]. Secondly, the radar antenna systems at the mentioned low MW frequencies are quite bulky which may abstain to be integrated with modern real-life compact devices like smart phones and tablets [23]. Ka band frequencies have also been investigated for RVSM to enhance the RVSM sensors sensitivity due to comparatively shorter wavelength at Ka frequencies [24–26].

In the recent years, millimetre-wave (MMW) frequencies (30–300 GHz) have drawn a remarkable research interest for RVSM implications [23, 27–35]. The main motives of RVSM at MMW frequencies include (i) improvement in the detection accuracy by employing shorter wavelength of the signal, (ii) smaller form factor for the device compactness and (iii) possibility of more subject focused signal transmission and reception to avoid the interference from the unwanted side reflections [22, 33–35]. From MMW band, 60 GHz band (57–66 GHz) has drawn more attraction because this band is free of licence and is quite mature due to its extensive use for several other wireless services [27].

Antenna designing for Doppler radar plays a crucial role in the precision of RVSM. The antenna should be designed in such a way that it only focuses the radiation beam on the subject [22] and should have an adequate gain to maintain a required signal to noise ratio [31]. Microstrip patch antennas are thought to better option for compact MMW sensors due to their embedment with on-chip devices, low profile, low cost and ability to make array to attain high antenna gain [23, 30–32]. In [30], conventionally designed microstrip patch antennas are integrated with on-chip micro-radar system for RVSM. However, the narrow microstrip transmission line (TL) designed for impedance matching and feeding purpose is fabricated with flip-chip method. In [31], two circularly polarised patch antenna arrays of elements have been presented for vital sign detection at 55 GHz. The antenna arrays and the associated narrow feed lines were fabricated by using special technique based on multilayer low-temperature co-fire ceramic (LTCC) substrate. The antennas gain remained as low as 4.86 dBi in case of two-element and 9.7 dBi in four-element arrays. Furthermore, for RVSM with these arrays, the subject has to hold breathing for a while for accurate detection of HR. Therefore, regarding RVSM at 60 GHz, there are still some gaps in the literature, i.e. cost-effective microstrip antenna arrays designed for accurate and simultaneous detection of BR and HR and the study of RVSM with single antenna for a very short distance and with double antennas for long distances.

In the present paper, three microstrip antenna arrays of ultra-wide elements have been designed for accurate detection of human BR and HR at 60 GHz band frequencies. The use of array antenna is made to minimise the interferences of the reflected signals from the side

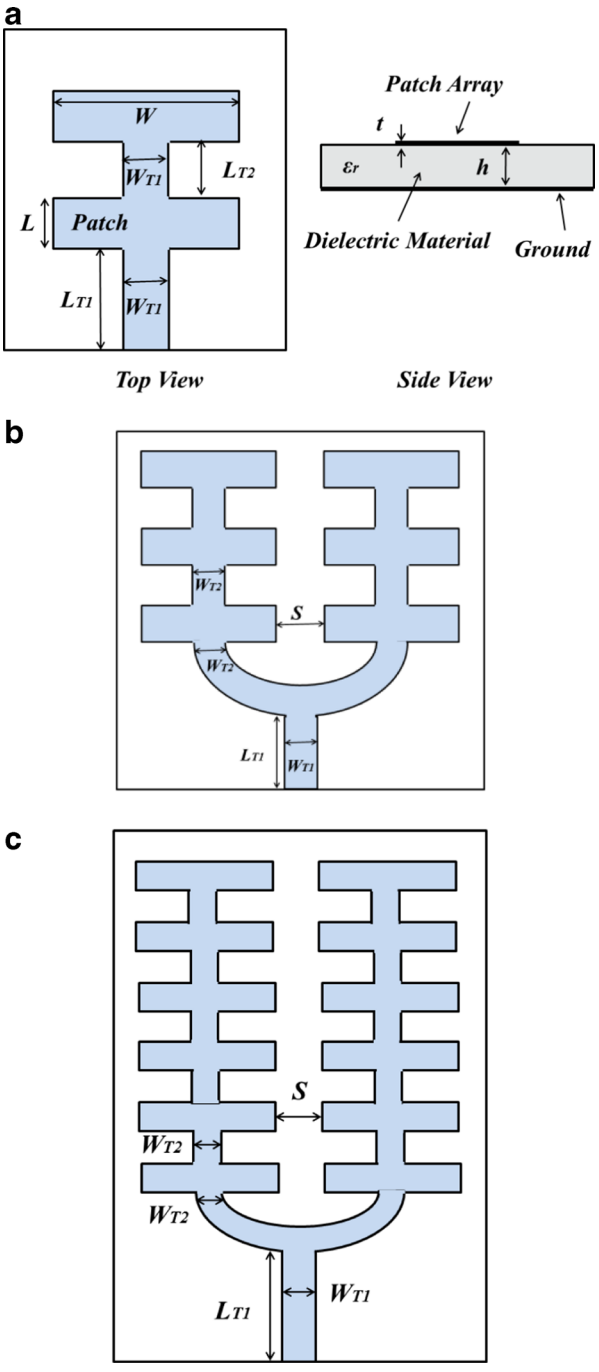

Fig. 1 Structures of the designed antenna arrays with (**a**) 2 × 1, (**b**) 3 × 2 and (**c**) 6 × 2 patch elements

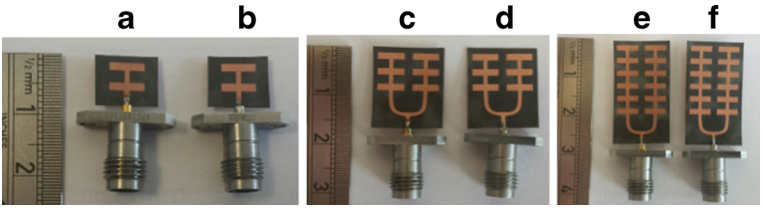

Fig. 2 Fabricated antenna arrays with (*a*)-(*b*) 2 × 1, (*c*)-(*d*) 3 × 2 and (*e*)-(*f*) 6 × 2 patch elements

objects because the array antennas have narrower radiation beamwidths than the single patch antenna [36]. Suitability of 60 GHz band for RVSM has been studied under the Doppler radar principle. Both BR and HR have been simultaneously measured of the subject sitting in front of the antennas and having normal breathing. The detection process has been studied in two ways: (i) with a single antenna used for both transmission and reception and (ii) with dual antennas, one for transmission and the other for reception. The ultra-wide patch elements provided a good trade-off between the arrays gain and size. The low side-lob levels, high gains, and narrow beam widths of the arrays confined the EM wave on the subject chest and ultimately improved the accuracy of RVSM. Moreover, all of the array dimensions were wide enough for conventional cost-effective fabrication with the ordinary PCB etching technology.

2 Antenna Design

Three microstrip patch antenna arrays have been designed at 60 GHz band on low loss Duroid substrate with thickness $h = 254\mu m$ and dielectric constant $\varepsilon_r = 2.2$. The structure diagrams of the arrays are presented in Fig. 1 where the arrays in Fig. 1a–c are comprised of 2 × 1, 3 × 2 and 6 × 2 patch elements, respectively.

The patch width (W) and length (L) are calculated as [37]:

$$W = \frac{\lambda_0 (2M+1)}{2\sqrt{\frac{\varepsilon_r + 1}{2}}} \tag{1}$$

$$L = \frac{\lambda_g (2N+1)}{2\sqrt{\varepsilon_{reff}}} - 2\Delta L \tag{2}$$

Where M and N are non-negative integers (in the current case $M = 1$ and $N = 0$) and λ_0 and λ_g are free space and guided wavelengths, respectively. ε_r and ε_{reff} are relative and effective

Table 1 Dimensions (mm) of the fabricated arrays

	L	W	L_{T1}	L_{T2}	W_{T1}	W_{T2}	S
Ant. 2(a)	1.34	5.1	1.88	2.42	0.86	0.86	0
Ant. 2(c)	1.45	5.47	1.73	2.37	0.9	0.7	1.58
Ant. 2(e)	1.45	5.47	2.13	2.39	0.93	0.75	2

dielectric constants, respectively. ΔL is the patch length extension due to the fringing field effect [38].

The specified patch width extension (i.e. $M = 1$in Eq. (1)) is adopted to improve the arrays gain by round 3 dB as compared to the gain of an array with conventional patch width (i.e. $M = 0$) [37]. Secondly, by employing the ultra-wide patches, the antenna's input impedance is

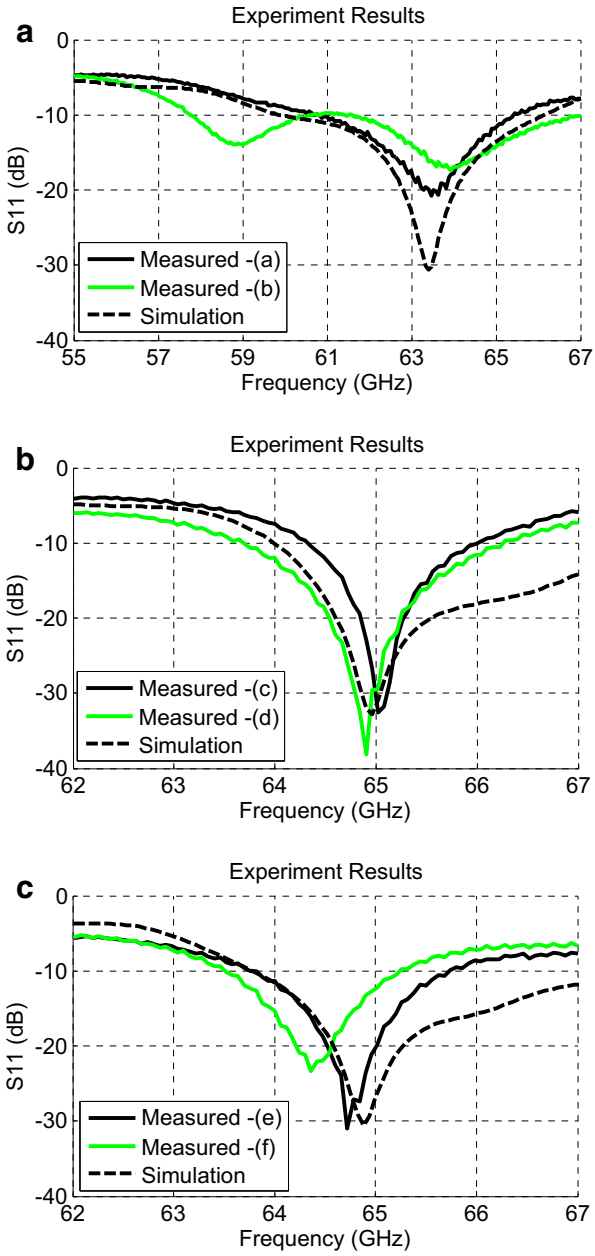

Fig. 3 Measured and simulation S_{11} of antenna arrays shown (**a**) in Fig. 2(*a*)-(*b*), (**b**) in Fig. 2(*c*)-(*d*) and (**c**) in Fig. 2(*e*)-(*f*)

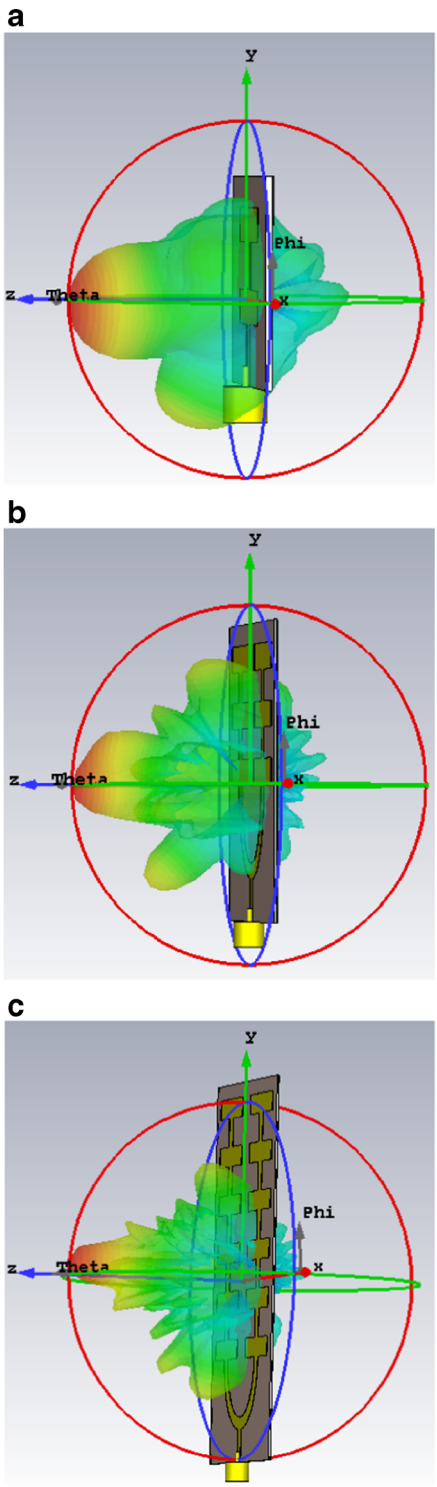

Fig. 4 Simulation 3-D FFPs of antenna arrays shown (**a**) in Fig. 2(*a*)-(*b*), (**b**) in Fig. 2(*c*)-(*d*) and (**c**) in Fig. 2(*e*)-(*f*)

reduced which ultimately helps to widen the feeding TL and hence to improve the fabrication tolerance should the conventional low cost PCB etching method be employed [37].

The TL length 'L_{T1}' is deployed as impedance transformer which is given as $L_{T1} = (2P + 1) \times \lambda/4$, where P is non-negative integer (in the current case $P = 1$). The inter-separations between the series and parallel patch elements are set to be $L_{T2} = \lambda_g/2 + 2\,\Delta L$ and $S = \lambda_g/2$, respectively (see Fig. 1), to match the current phase on the patch elements.

The TL width (W_{T1}) is computed based on the total input impedance (Z_a) of the array with n number of symmetrical patch elements [37]. A general expression for Z_a is

$$Z_a = \frac{59.81\lambda_0}{nW} \tag{3}$$

Z_a is matched with the standard 50Ω impedance through TL 'L_{T1}' with the characteristic impedance $Z_1 = \sqrt{50 \times Z_a}$.

The TL width (W_{T2}) is computed based on the total input impedance (Z_2) of the series patch elements in a line on one side of the array. The characteristic impedance of the line width 'W_{T2}' is given as $Z_2 = 59.81\lambda_0/(\mathrm{mW})$, where m is number of patch elements in series. The following is the general expression used to calculate the TL width W_T for the characteristic impedance Z [39]:

$$W_T = \frac{7.475\,h}{e^x} - 1.25t \tag{4}$$

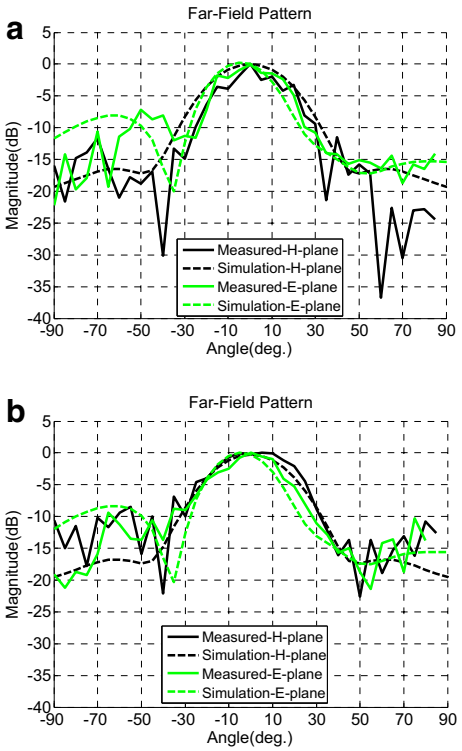

Fig. 5 Measured and simulation FFP of antenna arrays shown **a** in Fig. 2(*a*) and **b** in Fig. 2(*b*)

where $x = Z\sqrt{\varepsilon_r + 1.41}/87$ and t is copper cladding (see Fig. 1a).The final dimensions of the arrays are optimised with CST microwave studio for the best antenna performance.

3 Antenna Arrays Results

Figure 2 demonstrates the fabricated antenna arrays where (a)-(b), (c)-(d) and (e)-(f) are two copies of the array with 2 × 1, 3 × 2 and 6 × 2 number of patch elements, respectively.

Table 1 shows the dimensions of the fabricated arrays where it can be seen that all of the arrays dimensions are well above the PCB etching limit of 152-μm line width/gap.

Figure 3a–c illustrate the simulation and measured return loss responses of the arrays shown in Fig. 2(*a*)-(*b*), (*c*)-(*d*) and (*e*)-(*f*). As it can be seen from Fig. 3, the resonances of antennas 2(a)-(b) are centred at around 63.4 GHz and that of antennas 2(c)-(f) are centred in the range of 64.5 to 65 GHz but are better than −15 dB at 64.8 GHz. Therefore, 63.4 and 64.8 GHz frequency tones have been respectively selected for the RVSM when antennas 2(a)-(b) and 2(c)-(f) are employed.

Figure 4a–c present the simulated far-field patterns (FFP) in 3-D of the antennas shown in Fig. 2(*a*)-(*b*), (*c*)-(*d*) and (*e*)-(*f*), respectively, whereas Figs. 5, 6 and 7 respectively show their simulation and measured far-field patterns (FFP) in H and E planes at their selected frequencies as mentioned in the last paragraph. All of the antennas measured S_{11} and FFP results are within the PCB fabrication limit of 5% [31]. Some distortions in the antennas FFP in Figs. 6 and 7 can be observed which are due to the reflections from the surroundings and test fixtures [40]. It can

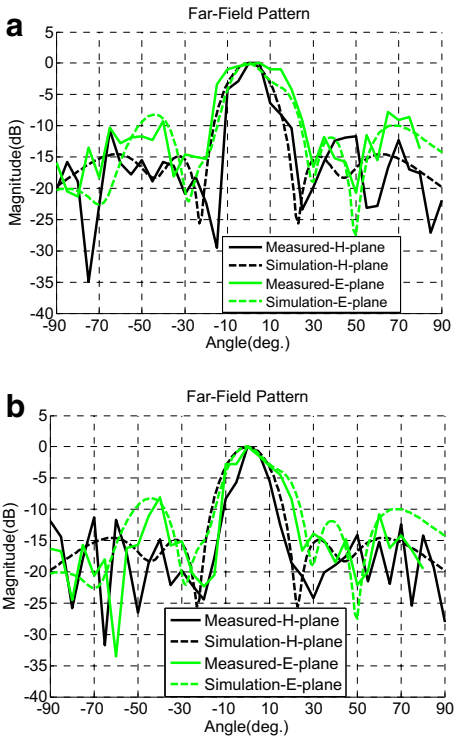

Fig. 6 Measured and simulation FFP of antenna arrays shown **a** in Fig. 2(*c*) and **b** in Fig. 2(*d*)

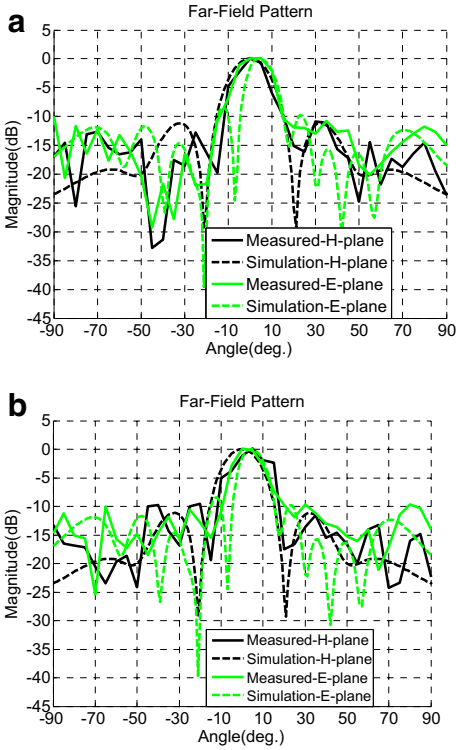

Fig. 7 Measured and simulation FFP of antenna arrays shown **a** in Fig. 2(*e*) and **b** in Fig. 2(*f*)

be noticed from Figs. 4, 5, 6 and 7 that the antennas' main lobs in the radiation patterns are directed almost towards 0° in both E and H planes for all the cases. The antennas' measured −10 dB return loss bandwidths (BW) and gains are summarised in Table 2 where it is obvious that gain of the arrays has significantly improved when more patch elements have used but the BW has reduced. However, the BW is not crucial for our current application of RVSM because only a single tone frequency will be used for the detection process.

4 Applicability of 60 GHz Doppler Radar for RVSM

Figure 8 shows the block diagram of various stages of RVSM process when Doppler radar principle is used for the vital signs detection. A single frequency tone of continuous electromagnetic wave (CW) is transmitted through a transmitter (T_x) antenna. The wave is reflected back from the subject chest located at a certain distance '*d*' and is received by a receiver (R_x) antenna. The quasi-periodic vibration of chest due to respiration and heat beat is phase

Table 2 Performance of antenna arrays shown in Fig. 2(*a*)-(*f*)

Ant.	(a)	(b)	(c)	(d)	(e)	(f)
BW (GHz)	4.62	5.52	1.68	2.57	1.9	1.73
Gain (dBi)	13.4	13.5	16	16.15	18.2	18.55

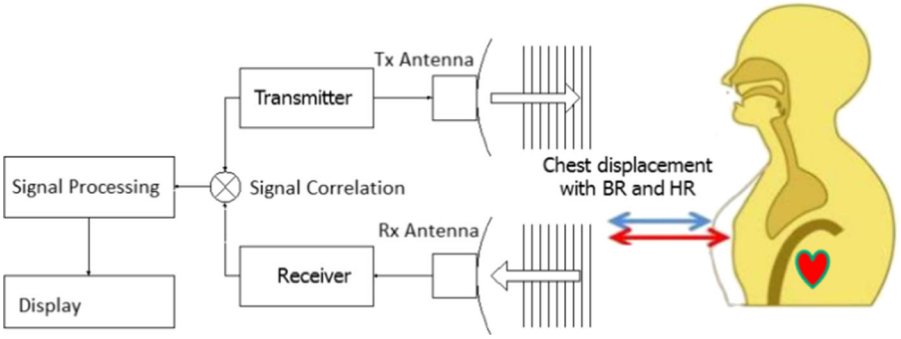

Fig. 8 Block diagram of RVSM process

modulated on the received signal. This phase-modulated signal at the R_x is correlated with transmitted signal and the outcome data is recorder for a certain period of time. Subsequently, the recorded raw data which is in time domain is processed through various signal processing techniques, i.e. digital filtering and Fourier Transformation, to extract the respiration and heart beat rate of the subject.

According to the Doppler radar theory, for a transmitted signal $S(t) = \cos(2\pi ft + \varphi(t))$, where f and $\varphi(t)$ are the frequency and phase noise of the transmitted wave, respectively, the received base band signal $R(t)$ may be approximated as [41]:

$$R(t) = \cos\left[\theta(t) + \frac{4\pi x_b(t)}{\lambda} + \frac{4\pi x_h(t)}{\lambda}\right] \tag{5}$$

where $\theta(t)$ is the total phase shift due to the signal path (d), reflections from the subject and surroundings and residual phase noise. λ, $x_b(t)$ and $x_h(t)$ are the operating wavelength, chest vibration displacement due to respiration and heartbeat, respectively. Due to the periodic nature of the $x_b(t)$ and $x_h(t)$, they may be approximated as $x_b(t) = m_b \sin(2\pi f_b t)$ and $x_h(t) = m_h \sin(2\pi f_h t)$, where m_b and m_h are the displacement amplitudes of the chest motion due to respiration and heartbeat, respectively. f_b and f_h are the frequencies of BR and HR, respectively. This way, the expansion of Eq. (4) in Fourier series leads to [24]:

$$R(t) = \sum_{i=-\infty}^{\infty}\sum_{j=-\infty}^{\infty} J_j\left[\frac{4\pi m_b}{\lambda}\right] J_i\left[\frac{4\pi m_h}{\lambda}\right] \cos(j\ \ 2\pi f_b t + i\ \ 2\pi f_h t + \theta) \tag{6}$$

Where $J_n(X)$ is Bessel function of first kind with argument X. Taking the first positive harmonics of both f_b and f_h into account, the above equation can be written as

$$\begin{aligned} R(t) = {} & J_1\left[\frac{4\pi m_b}{\lambda}\right] J_0\left[\frac{4\pi m_h}{\lambda}\right] \cos(2\pi f_b t + \theta) \\ & + J_0\left[\frac{4\pi m_b}{\lambda}\right] J_1\left[\frac{4\pi m_h}{\lambda}\right] \cos(2\pi f_h t + \theta) \end{aligned} \tag{7}$$

where $J_1\left[\frac{4\pi m_b}{\lambda}\right] J_0\left[\frac{4\pi m_h}{\lambda}\right]$ and $J_0\left[\frac{4\pi m_b}{\lambda}\right] J_1\left[\frac{4\pi m_h}{\lambda}\right]$ are the amplitudes of the phase variations in

Fig. 9 **a** Plots of Bessel functions $J_0(X)$, $J_1(X)$ and their product $J_0(X) \times J_1(X)$ for argument X. Magnitude of the phase amplitude of $R(t)$ in Eq. (6) due to **b** both BR and HR in combined, **c** just BR signal and **d** just HR signal, for various combinations of m_b and m_h

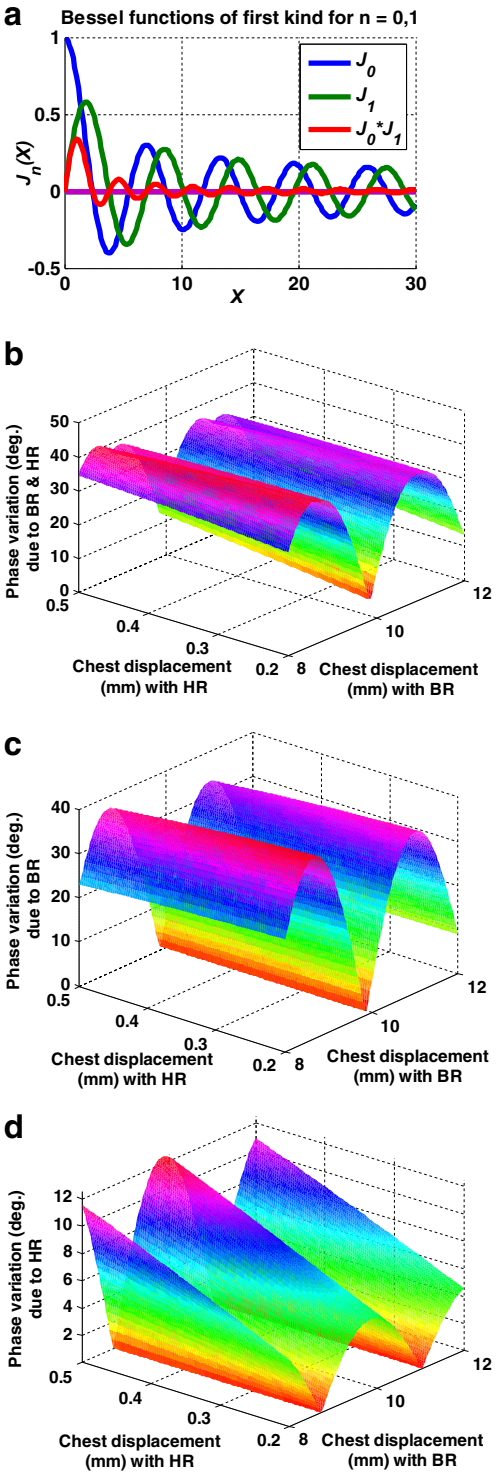
a
Bessel functions of first kind for n = 0,1
J0
J1
J0*J1
Jn(X)
X
b
Phase variation (deg.) due to BR & HR
Chest displacement (mm) with HR
Chest displacement (mm) with BR
c
Phase variation (deg.) due to BR
Chest displacement (mm) with HR
Chest displacement (mm) with BR
d
Phase variation (deg.) due to HR
Chest displacement (mm) with HR
Chest displacement (mm) with BR

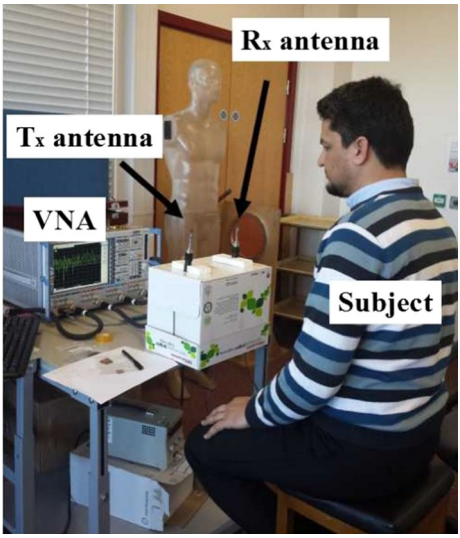

Fig. 10 Experiment setup to measure the RVSM at 60 GHz band

$R(t)$ due to respiration and heartbeat, respectively. Equation (6) contains the essential information related to the applicability of 60 GHz band frequencies for RVSM. Based on Eq. (6), we are going to analyse and visualise the key factors involved in RVSM at 60 GHz band.

Figure 9a shows the plots of $J_0(X)$, $J_1(X)$ and their product for the argument X up to 30 where it can be noticed that $J_0(X)$ and $J_1(X)$ are the periodic functions with some phase shift and the maximum amplitude of their product is much smaller than their individual maximum amplitudes and it passes through null values twice as compared to individual $J_0(X)$ and $J_1(X)$ curves. Furthermore, the amplitude of $J_0(X) \times J_1(X)$ diminishes for higher values of argument X. Now bearing Eq. (6) in mind, the amplitude of the received BR and HR signal is comprised of the product of $J_0(X)$ and $J_1(X)$ and the argument X is controlled by m_b, m_h and λ. For our current case of VSM at 60 GHz band, λ is around 4.65 mm, $m_b = (8 - 12)$mm and $m_r = (0.2 - 0.5)$mm for a person at rest with normal breathing [42]. Figure 9b–d shows the phase amplitude variations of $R(t)$ signal for various combination of m_b and m_r with BR and HR in combined, only BR and HR, respectively. From Fig. 9b, it can be seen that the maximum $R(t)$ amplitude goes to around 40° which is high enough for RVSM detection; however, there is a null detection line at chest amplitude of around 9.9 mm. Figure 9c indicates a similar null

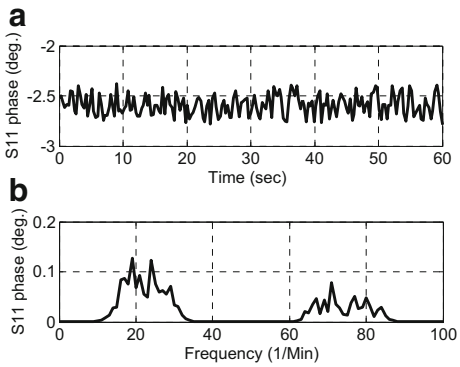

Fig. 11 RVSM measurement with antenna shown in Fig. 2(*a*). **a** Recorded raw data in time domain.**b** Detected BR and HR peaks

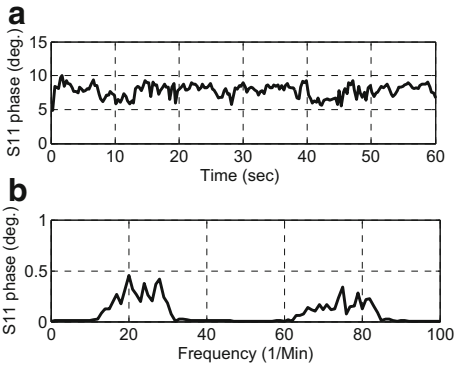

Fig. 12 RVSM measurement with antenna shown in Fig. 2(*c*). **a** Recorded raw data in time domain. **b** Detected BR and HR peaks

line position for just BR signal. On the other hand, Fig. 9d shows that in case of the received HR signal, there are two null detection lines at chest displacements of 8.8 and 11 mm and the maximum phase amplitude of heartbeat is about one third of that of respiration. However, the probability of these undesired m_b and m_h combinations and hence the null detection points is very low and a small variation in λ can be made to avoid these points (see Eq. (6)) [24]. As a conclusion so far, both BR and HR signals have high probability of detection with RVSM at 60 GHz band but the received BR signal may be clearer than HR signal.

5 RVSM Results and Discussions

Figure 10 shows the experiment setup to measure the RVSM at 60 GHz band. The 67 GHz Rohde and Schwarz VNA is used as transmitter and receiver. The three antenna designs as presented in section III (see Fig. 2) have been employed one by one for signal transmission and reception. As mentioned in section I, for each antenna design, the RVSM data has been acquired with two ways; (i) with a single antenna employed for both transmission and reception and (ii) with double antennas (two similar antennas), one for transmission and the other for reception. A normally breathing person sits in front of the antennas iteratively at different distances (*d*) and the RVSM data is recorded for 60 s for each iteration. The recorded data is then processed in Matlab programme through various digital signal processing techniques and the targeted BR and HR have been extracted. The major parts of digital signal

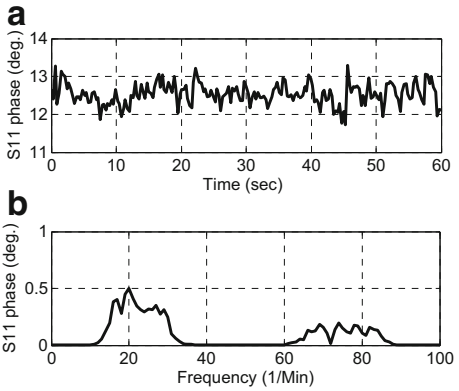

Fig. 13 RVSM measurement with antenna shown in Fig. 2(*e*). **a** Recorded raw data in time domain. **b** Detected BR and HR peaks

Table 3 Measured BR and HR with single antenna in Fig. 2

Antenna	2(a)	2(c)	2(e)
BR	19	20	20
HR	71	75	74

processing include digital filtering of the recorded raw data in time domain and Discrete Fast Fourier Transformation (DFFT) of the filtered data [43–46].

5.1 RVSM with Single Antenna

As mentioned earlier, in the single-antenna operation, only one of each designed antenna arrays is employed for both signal transmission and reception and the vital signs can only be accurately detected for very short distance [6]. The antenna is placed at about 5 cm away from the subject chest and the phase of the reflection coefficients (S_{11}), which contain the HR and BR information, has been recorded for 60 s. Figs. 11, 12 and 13 illustrate the measured RVSM data with the individual-antenna arrays shown in 2(a), (c) and (e), respectively. Figs. 11a, 12a and 13a represent the recorded raw data of S11 phase and Figs. 11b, 12b and 13b depict the DFFT of the processed data in frequency (1/min) domain. As seen from Figs. 11b, 12b and 13b, in each case, the first and the second highest peaks represent the detected BR and HR, respectively. All of the detected BR and HR are listed in Table 3 where it is obvious that both BR and HR are consistent within their respective ranges for the ordinary subject (31-year-old man) [47]. The measured BR and HR results are also matched with the results obtained with manual counting by using a stopwatch.

5.2 RVSM with Double Antennas

In RVSM with double antenna operation, two similar antennas are deployed for vital sign detection, one for transmitting the EM wave and the other for receiving the reflected wave. Both antennas are fixed at an equal distance from the subject chest with their main beams directed to the chest. The inter-separation between the antennas is set to be about 20 cm. The phase of S21 is recorded for 60 s for RVSM with each antenna design shown in Fig. 2(*a*)-(*f*). The accuracy of the RVSM has been studied for various distances (*d*) between the subject and antennas ranging from 25 to 200 cm. Figures 14, 15 and 16 demonstrate the RVSM data with antenna design 2(a)-(b) from distance 0.25, 1 and 2 m, respectively. Similarly, Figs. 17 and 18

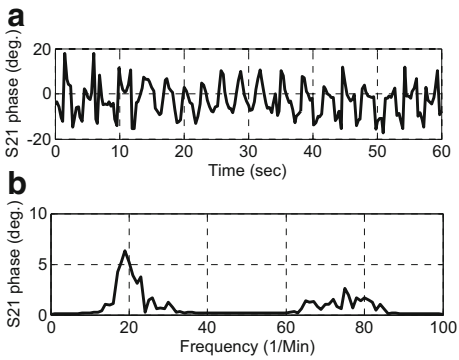

Fig. 14 RVSM measurement with antenna shown in Fig. 2(*a*)-(*b*) from 0.25 m. **a** Recorded raw data in time domain. **b** Detected BR and HR peaks

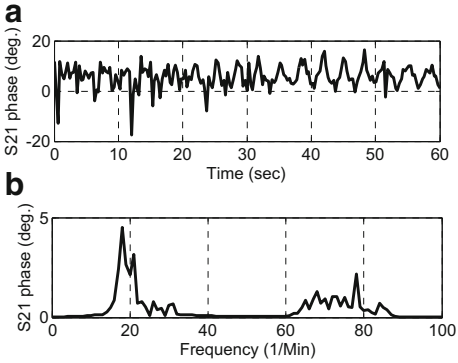

Fig. 15 RVSM measurement with antenna shown in Fig. 2(*a*)-(*b*) from 1 m. **a** Recorded raw data in time domain. **b** Detected BR and HR peaks

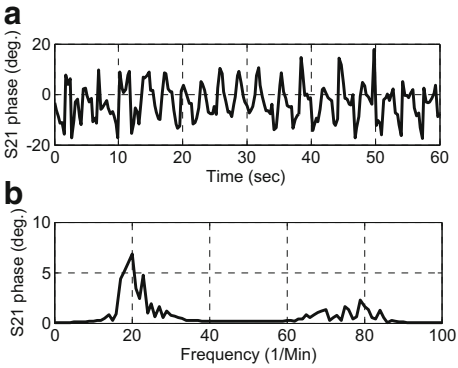

Fig. 16 RVSM measurement with antenna shown in Fig. 2(*a*)-(*b*) from 2 m. **a** Recorded raw data in time domain. **b** Detected BR and HR peaks

and Figs. 19 and 20 demonstrate the RVSM data with each antenna design 2(c)-(d) and 2(e)-(f) from distance 0.25 and 1 m, respectively. The sub-figs. (a) and (b) in Figs. 14, 15, 16, 17, 18, 19 and 20 represent the recorded raw data in time domain and the processed data in frequency (1/min) domain, respectively. The first and the second peak in the processed data in Figs. 14, 15, 16, 17, 18, 19 and 20 represent the measured BR and HR, respectively, where it can be seen that both BR and HR peaks are very obvious across the frequency spectrum. The measured BR and HR results of RVSM with dual antennas up to 1 m distances are shown

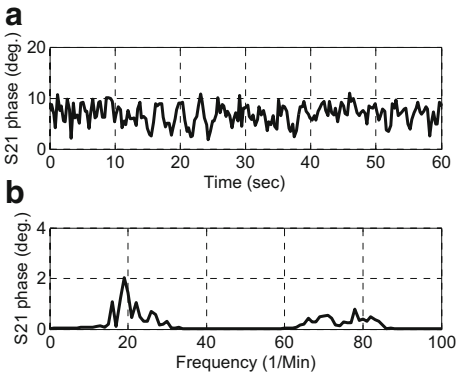

Fig. 17 RVSM measurement with antenna shown in Fig. 2(*c*)-(*d*) from 0.25 m. **a** Recorded raw data in time domain. **b** Detected BR and HR peaks

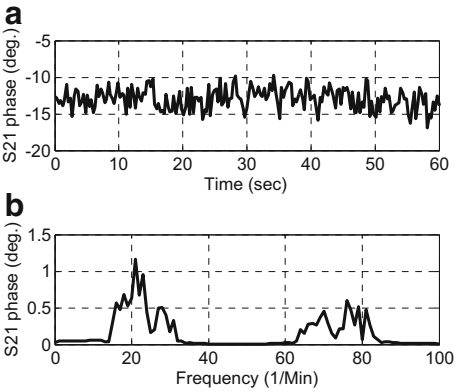

Fig. 18 RVSM measurement with antenna shown in Fig. 2(*c*)-(*d*) from 1 m. **a** Recorded raw data in time domain. **b** Detected BR and HR peaks

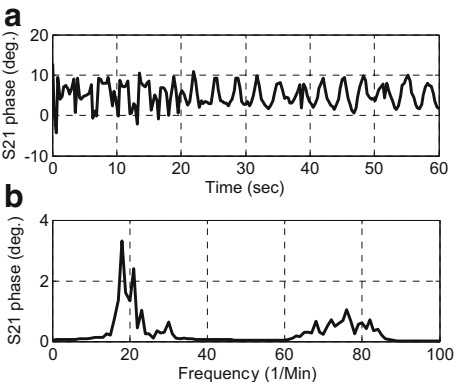

Fig. 19 RVSM measurement with antenna shown in Figs. 2(*e*)-(*f*) from 0.25 m. **a** Recorded raw data in time domain. **b** Detected BR and HR peaks

in Table 4. The detected BR and HR with antenna design 2(a)-(b) in case of 2 m distance are 19/min and 79/min, respectively. In all the cases, both BR and HR results are consistent within their expected ranges and are matched with the results obtained by manual counting as mentioned earlier.

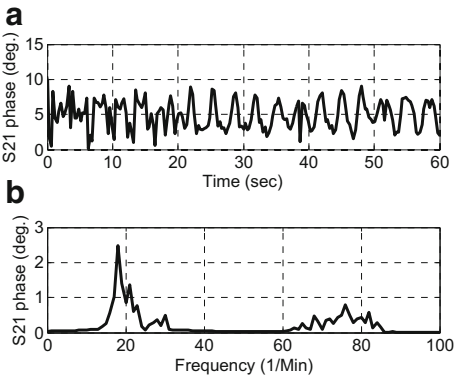

Fig. 20 RVSM measurement with antenna shown in Fig. 2(*e*)-(*f*) from 1 m. **a** Recorded raw data in time domain. **b** Detected BR and HR peaks

Table 4 Measured BR and HR with dual antennas

	Antenna 2(a)-(b)	Antenna 2(c)-(d)	Antenna 2(e)-(f)
d	BR-HR	BR-HR	BR-HR
0.25 m	19–75	19–78	18–76
1 m	18–78	21–76	18–72

6 Conclusion

Three microstrip antenna arrays have been designed based on ultra-wide patch elements with improved gain and radiation characteristics for accurate RVSM at 60 GHz band frequencies. The antenna simulation and measured results agreed well in all cases. The feasibility of 60 GHz channel has been studied for RVSM application under the Doppler radar principle. The RVSM measurements have been conducted with each designed array in (i) single-antenna operation, where the same antenna working as T_x and R_x is placed at 5 cm from the subject chest, as well as (ii) in double antennas operation where two identical antennas, one for T_x and the other for R_x, have been deployed at various distances from the subject to see the consistency in the results accuracy. Both BR and HR have been detected for the subject with normal breathing throughout the data recording time and no breath holding was required for accurate HR detection. In all of the cases, the measured results showed very accurate, clear and robust detection of RVSM with simple digital signal processing techniques. For future work, the proposed antenna arrays could be used for outdoor RVSM detection from even longer distance. Furthermore, the potential error sources like the signal reflections from the side objects through the antennas' side lobes, accuracy of the vital signs of the diversity of patient types can be investigated in details.

References

1. L. Sun, Y. Li, H. Hong, F. Xi, W. Cai, X. Zhu, Super-resolution spectral estimation in short-time non-contact vital sign measurement, Review of Scientific Instruments, 2015 Apr 1;86(4):044708
2. A. D. Droitcour, T. B. Seto, B-K. Park, S. Yamada, A. Vergara, C. E. Hourani, T. Shing, A.Yuen, V. M. Lubecke, and O. Boric-Lubecke, Non-contact respiratory rate measurement validation for hospitalized patients, In 2009 Annual International Conference of the IEEE Engineering in Medicine and Biology Society, pp. 4812-4815. IEEE, (2009)
3. M. Villarroel, A. Guazzi, J. Jorge, S. Davis, P. Watkinson, G. Green, A. Shenvi, K. McCormick, and L. Tarassenko, Continuous non-contact vital sign monitoring in neonatal intensive care unit, *Healthcare technology letters* 1, no. 3 (2014): 87
4. S. Suzuki, T. Matsui, M. Kagawa, T. Asao, and K. Kotani, An approach to a non-contact vital sign monitoring using dual-frequency microwave radars for elderly care, Journal of Biomedical Science and Engineering 6, no. 07 (2013): 704
5. M. Uenoyama, T. Matsui, K. Yamada, S. Suzuki, B. Takase, S. Suzuki, M. Ishihara, and M. Kawakami, Non-contact respiratory monitoring system using a ceiling-attached microwave antenna, *Medical and Biological Engineering and Computing* 44, no. 9 (2006): 835-840

6. D. Obeid, G. Zaharia, S. Sadek and G. El Zein, 2012. Microwave doppler radar for heartbeat detection vs electrocardiogram. Microwave and Optical Technology Letters, 54(11), pp.2610-2617.
7. Kao, T.Y.J. and Lin, J., 2013, April. Vital sign detection using 60-GHz Doppler radar system. In Wireless Symposium (IWS), 2013 I.E. International (pp. 1-4). IEEE.
8. C. Gu, Short-Range Noncontact Sensors for Healthcare and Other Emerging Applications: A Review. Sensors, 16(8), 2016, p.1169.
9. L. Ren, Y. S. Koo, H. Wang, Y. Wang, Q. Liu, A. E. Fathy, Noncontact Multiple Heartbeats Detection and Subject Localization Using UWB Impulse Doppler Radar, *IEEE Microwave and Wireless Components Letters* 25, no. 10 (2015): 690-692
10. F. Adib, H. Mao, Z. Kabelac, D. Katabi and R. C. Miller, Smart homes that monitor breathing and heart rate, In *Proceedings of the 33rd Annual ACM Conference on Human Factors in Computing Systems*, pp. 837-846. ACM, (2015)
11. S. Suzuki, T. Matsui, H. Kawahara, H. Ichiki, J. Shimizu, Y. Kondo, S. Gotoh, H. Yura, B. Takase and M. Ishihara, A non-contact vital sign monitoring system for ambulances using dual-frequency microwave radars, *Medical & biological engineering & computing* 47, no. 1 (2009): 101-105
12. C. Brüser, C. H. Antink, T. Wartzek, M. Walter, and S. Leonhardt, Ambient and Unobtrusive Cardiorespiratory Monitoring Techniques, *IEEE reviews in biomedical engineering* 8 (2015): 30-43
13. C. Li, Y. Xiao and J. Lin, A 5GHz Double-Sideband Radar Sensor Chip in 0.18 m CMOS for Non-Contact Vital Sign Detection, *IEEE Microwave and Wireless Components Letters* 18, no. 7 (2008): 494-496
14. S. Kazemi, A. Ghorbani, H. Amindavar and D. R. Morgan, Vital-Sign Extraction Using Bootstrap-Based Generalized Warblet Transform in Heart and Respiration Monitoring Radar System, *IEEE Transactions on Instrumentation and Measurement* 65, no. 2 (2016): 255-263.
15. A. D. Droitcour, O. Boric-Lubecke, V. M. Lubecke, J. E. N. S. H. A. N. Lin and G. T. A. Kovacs, Range correlation effect on ISM band I/Q CMOS radar for non-contact vital signs sensing, In *Microwave Symposium Digest, 2003 I.E. MTT-S International*, vol. 3, pp. 1945-1948. IEEE, (2003)
16. M-C. Huang, J. J. Liu, W. Xu, C. Gu, C. Li, and M. Sarrafzadeh, A self-calibrating radar sensor system for measuring vital signs, *IEEE transactions on biomedical circuits and systems* 10, no. 2 (2016): 352-363.
17. μm CMOS for non-contact vital sign detection, In *2009 I.E. Radio Frequency Integrated Circuits Symposium*, pp. 97-100. IEEE, (2009)
18. C. Li, Y. Xiao and J. Lin, Design guidelines for radio frequency non-contact vital sign detection, In *2007 29th Annual International Conference of the IEEE Engineering in Medicine and Biology Society*, pp. 1651-1654. IEEE, (2007)
19. C. Li and J. Lin, Complex signal demodulation and random body movement cancellation techniques for non-contact vital sign detection, In *Microwave Symposium Digest, 2008 I.E. MTT-S International*, pp. 567-570. IEEE, (2008)
20. C. Li, J. Ling, J. Li and J. Lin, Accurate Doppler radar noncontact vital sign detection using the RELAX algorithm, *IEEE Transactions on Instrumentation and Measurement* 59, no. 3 (2010): 687-695
21. Rahman, E. Yavari, X. Gao, V. Lubecke and O. Boric-Lubecke, Signal processing techniques for vital sign monitoring using mobile short range Doppler radar, In *Biomedical Wireless Technologies, Networks, and Sensing Systems (BioWireleSS), 2015 I.E. Topical Conference on*, pp. 1-3. IEEE, (2015)
22. C. Li, V. M. Lubecke, O. Boric-Lubecke and J. Lin, A review on recent advances in Doppler radar sensors for noncontact healthcare monitoring, *IEEE Transactions on microwave theory and techniques* 61, no. 5 (2013): 2046-2060
23. T-Y. J. Kao, A. Y-K. Chen, Y. Yan, T-M. Shen and J. Lin, A flip-chip-packaged and fully integrated 60 GHz CMOS micro-radar sensor for heartbeat and mechanical vibration detections, In *2012 I.E. Radio Frequency Integrated Circuits Symposium*, pp. 443-446. IEEE, (2012)
24. C. Li and J. Lin, Optimal carrier frequency of non-contact vital sign detectors, In *2007 I.E. Radio and Wireless Symposium*, pp. 281-284. IEEE, (2007)
25. C. Li and J. Lin, Non-contact measurement of periodic movements by a 22-40GHz radar sensor using nonlinear phase modulation, In *2007 IEEE/MTT-S International Microwave Symposium*, pp. 579-582. IEEE, (2007)
26. N. Birsan and D-P. Munteanu, Non-contact cardiopulmonary monitoring algorithm for a 24 GHz Doppler radar, In *2012 Annual International Conference of the IEEE Engineering in Medicine and Biology Society*, pp. 3227-3230. IEEE, 2012
27. H-R. Chuang, H-C. Kuo, F-L. Lin, T-H. Huang, C-S. Kuo and Y-W. Ou, 60-GHz millimeter-wave life detection system (MLDS) for noncontact human vital-signal monitoring, *IEEE Sensors Journal* 12, no. 3 (2012): 602-609.
28. H-C. Kuo, H-H. Wang, P-C. Wang, H-R. Chuang, and F-L. Lin, 60-GHz millimeter-wave life detection system with clutter canceller for remote human vital-signal sensing, In *Microwave Workshop Series on Millimeter Wave Integration Technologies (IMWS), 2011 I.E. MTT-S International*, pp. 93-96. IEEE, (2011)

29. H-C. Kuo and H-R. Chuang, Investigation of carrier frequency effect on detection performance of Doppler sensor systems for noncontact human vital-signs sensing, In *2014 8th International Symposium on Medical Information and Communication Technology (ISMICT)*, pp. 1-4. IEEE, (2014)
30. T-Y. J. Kao, Y. Yan, T-M. Shen, A. Y-K. Chen and J. Lin, Design and analysis of a 60-GHz CMOS Doppler micro-radar system-in-package for vital-sign and vibration detection, *IEEE Transactions on Microwave Theory and Techniques* 61, no. 4 (2013): 1649-1659
31. T-M. Shen, T-Y. J. Kao, T-Y. Huang, J. Tu, J. Lin and R-B. Wu, Antenna design of 60-GHz micro-radar system-in-package for noncontact vital sign detection, *IEEE Antennas and Wireless Propagation Letters* 11 (2012): 1702-1705
32. J. Gao, K. Li, T. Sato, J. Wang, H. Harada S. and Kato, January. Implementation considerations of patch antenna array for 60GHz beam steering system applications. In 2009 I.E. Radio and Wireless Symposium(pp. 35-38). IEEE, 2009
33. Bakhtiari, Sasan, Thomas W. Elmer, Nicholas M. Cox, Nachappa Gopalsami, Appostolos C. Raptis, Shaolin Liao, Ilya Mikhelson, and Alan V. Sahakian. "Compact millimeter-wave sensor for remote monitoring of vital signs." *IEEE Transactions on Instrumentation and Measurement* 61, no. 3 (2012): 830-841.
34. S. Bakhtiari, S. Liao, T. Elmer and A. C. Raptis, A real-time heart rate analysis for a remote millimeter wave IQ sensor, *IEEE Transactions on Biomedical Engineering* 58, no. 6 (2011): 1839-1845
35. D. T. Petkie, C. Benton and E. Bryan, Millimeter wave radar for remote measurement of vital signs, (2009): 1.
36. Yang, Z., Pathak, P.H., Zeng, Y., Liran, X. and Mohapatra, P., Monitoring Vital Signs Using Millimeter Wave. DOI: http://dx.doi.org/10.1145/2942358.2942381 [Online] Available at: [http://www.phpathak.com/files/mmvital-mobihoc.pdf], accessed on October the 1th, 2016
37. M. S. Rabbani and H. Ghafouri-Shiraz, Size improvement of rectangular microstrip patch antenna at MM-wave and terahertz frequencies, Microwave and Optical Technology Letters 57, no. 11 (2015): 2585-258937
38. R. Bancroft, Microstrip and printed antenna design [electronic resource]. Raleigh, NC, SciTech Pub. (2009)
39. Analog Devices, MT-094: Microstrip and Stripline Design - Analog Devices, [Online] Available at: http://www.analog.com/static/imported-files/tutorials/MT-094.pdf, accessed on July the 7th, 2016
40. M. S. Rabbani, and H. Ghafouri-Shiraz, Improvement of Microstrip Patch Antenna Gain and Bandwidth at 60GHz and X Bands for Wireless Application, IET Microwaves, Antennas & Propagation, DOI: 10.1049/iet-map.2015.0672, 2016.
41. C. Gu, C. Li, J. Lin, J. Long, J. Huangfu and L Ran, Instrument-based noncontact Doppler radar vital sign detection system using heterodyne digital quadrature demodulation architecture, *IEEE Transactions on Instrumentation and Measurement* 59, no. 6 (2010): 1580-1588
42. D. Obeid, S. Sadek, G. Zaharia, and G. E. Zein, Multitunable microwave system for touchless heartbeat detection and heart rate variability extraction, Microw. Opt. Technol. Lett., 52: 192–198. doi: 10.1002/mop.24877, (2010)
43. M. Valipour, Optimization of neural networks for precipitation analysis in a humid region to detect drought and wet year alarms. *Meteorological Applications*, *23*(1), 2016, pp.91-100.
44. M. Valipour, M. E. Banihabib and S. M. R. Behbahani, Comparison of the ARMA, ARIMA, and the autoregressive artificial neural network models in forecasting the monthly inflow of Dez dam reservoir. *Journal of hydrology*,*476*, 2013, pp.433-441.
45. M. Valipour, M. A. G. Sefidkouhi and S. Eslamian, Surface irrigation simulation models: a review. *International Journal of Hydrology Science and Technology*, *5*(1), 2015, pp.51-70.
46. M. Valipour, Sprinkle and trickle irrigation system design using tapered pipes for pressure loss adjusting. *Journal of Agricultural Science*,*4*(12), 2012, p.125
47. NHS. Online at: http://www.nhs.uk/chq/Pages/2024.aspx, accessed on July the 7th, 2016